S. Foletti,[1] S. Beretta,[1] F. Scaccabarozzi,[1] S. Rabbolini,[1] and L. Traversone[2]

Fatigue Crack Growth in Blade Attachment of Turbine Disks: Experimental Tests and Life Prediction

Manuscript received March 5, 2014; accepted for publication August 14, 2014; published online September 26, 2014.

[1] Politecnico Di Milano, Dipartimento di Meccanica, Via La Masa 1, 20156 Milano, Italy.

[2] AEN Ansaldo Energia, Via Lorenzi 8, 16152 Genova, Italy.

Nomenclature

$2c$ = surface crack length (mm)
A_0, dA_n = plastic zone area at the crack tip projected on the ligament (mm^2)
a, Δa, a_i = crack depth (mm)
a_0 = initial radius of defect (mm)
BL = base load condition (nominal speed of the turbine)
C_{07}, n_{07} = parameters of long crack propagation Paris curve at $R = 0.7$
da/dn, dc/dn = crack growth rate (mm/cycle)
f = closure factor
F = force in the load direction (kN)
h = Wang–Lambert weight function
H_i = Newman expressions coefficients
K, ΔK = stress intensity factor ($MPam^{0.5}$)
K_A = stress intensity factor at the deepest point A of the crack ($MPam^{0.5}$)
K_C = stress intensity factor at the surface point C of the crack ($MPam^{0.5}$)
K_{max} = maximum stress intensity factor during loading ($MPam^{0.5}$)
K_{min} = minimum stress intensity factor during loading ($MPam^{0.5}$)
K_0 = flow stress intensity factor ($MPam^{0.5}$)
K_{op} = opening stress intensity factor ($MPam^{0.5}$)
OL = load case corresponding to turbine overspeed
OL + BL = load case corresponding to overspeed followed by baseload cycles
$PEEQ$ = equivalent plastic strain
R = load ratio
R_m = ultimate tensile strength (MPa)
$R_{p,02}$ = yield stress (0.2 % offset)(MPa)
α = constraint factor
Δa_{nuc} = crack variation due to nucleation (mm)
ΔK_{eff} = effective Stress Intensity Factor range ($MPam^{0.5}$)
ε = strain in the load direction (mm/mm)
$\varepsilon_{\max}$ = maximal principal strain (mm/mm)
σ_0 = flow stress (MPa)
$\sigma_{\max}$ = maximal principal stress (MPa)
σ_n = stress in the plastic zone (MPa)
σ_p = opening stress (MPa)
$\sigma_{VM,\max}$ = maximal von Mises stress (MPa)

Introduction

The main reason for the proliferation of gas turbines to drive an electric generator is the low time required to reach the base-load condition. Nowadays, turbogas plants are widely used to meet the peak loads requested by users; as a consequence, each plant component withstands, in its lifetime, several start-up and shut-down cycles,

up to 20 000 cycles without significant maintenance actions. This cyclic loading may induce plastic deformations in some critical regions of the components such as notches.

Regarding design of massive components of turbines, such as disks and shafts, it is also necessary to consider that, due to the technological processes (forging and machining) and fretting damages, micro-defects and damages can be present inside the components. Accordingly, the correct approach to face the design problems of massive components is the "Flaw Tolerant" approach [1].

Before service, each machine is usually tested at a speed significantly higher than the nominal one, in order to test each component with a significant safety mar-gin. The initial overload may induce mechanical stresses greater than the yield stress and create a plastic zone in some critical points such as geometry notches. The mate-rial response to a subsequent load at 100 % of nominal speed is consequently differ-ent form the response of a component loaded only at nominal conditions, without first having endured an overload.

The aim of this paper is to analyze through both experimental and numeri-cal tools the high stress concentration at the root of blade attachments in the first compressor disks (negligible thermal load) of a real gas turbine and to an-alyze the behavior of a potential defect in these critical regions. Firstly, the stress field at the blade attachment region has been identified through a FE analysis of a sector of a real disk. To experimentally reproduce the identified stress-strain condition, "companion" notched specimens have been designed to represent the plastic zone field and the high stress concentration at the root of blade attachments. A series of experimental tests in the LCF regime, with and without the presence of the overload, has been carried out in presence of small semi-circular EDM micronotches. In particular, crack growth rate has been measured with the method of plastic replicas, as in Ref. [2]. Since the numeri-cal analyses and experimental tests have shown a condition of elastic shake-down at the root of notched specimens, the crack driving force could be expressed in terms of stress intensity factor, ΔK (SIF) [3]. The crack propaga-tion was then modeled through the Newman's closure function [4], while SIF was calculated through a weight function [5] and the stabilized elasto-plastic stress at the notch root.

The predictions correlate to the experimental crack growth data sufficiently well as to support the adoption of the crack propagation algorithm onto a software for life prediction of turbine rotor disks [6].

Design of Companion Specimens

STRESS STATE AT BLADE ATTACHMENT

In order to identify the most critical stress-strain condition in the blade attachment of a compressor disk of a gas turbine, a FE analysis of an angular section (1/33th symmetry) of the disk has been carried out (**Fig. 1(*a*)**) using Abaqus/CAE 6.11-2 soft-ware, with radial symmetry condition and an highly refined mesh near the blade attachment (**Fig. 1(*b*)**). In order to correctly represent material cyclic response at the first overyielding loads, material cyclic behavior has been modeled using a combined

cyclic elastic–plastic model, which considered both isotropic and kinematic hardening. The isotropic hardening has been assumed through the Voce equation [7], while the kinematic hardening has been modeled with the non-linear Chaboche model [8] with 5 backstresses.

The load steps have been set to reproduce the real load condition of the disks, considering the centrifugal load consequence of the rotational speed as the main load. The first step, as in **Fig. 1(c)**, implements the overspeed due to the spinning test (O→A→B), whereas the following cycles reproduce two start-ups and shut-downs at the nominal speed ($B \rightarrow A^I \rightarrow B^I$).

The results of the FE analysis of the disk are shown in **Fig. 2** (due to confidentiality, all the results have been normalized). The first overload creates a plastic strain field at the root of the blade attachment: the unloading is elastic so that re-sidual compression stresses are induced. Due to local stress field, the following loading cycles at nominal speed are completely elastic in an elastic shakedown con-dition [9].

FIG. 1 Finite element analysis of a real disk: (*a*) FE model, (*b*) refined mesh at the root of blade attachment, (*c*) load steps implemented for representing the initial overspeed (spinning test) followed by nominal speed cycles.

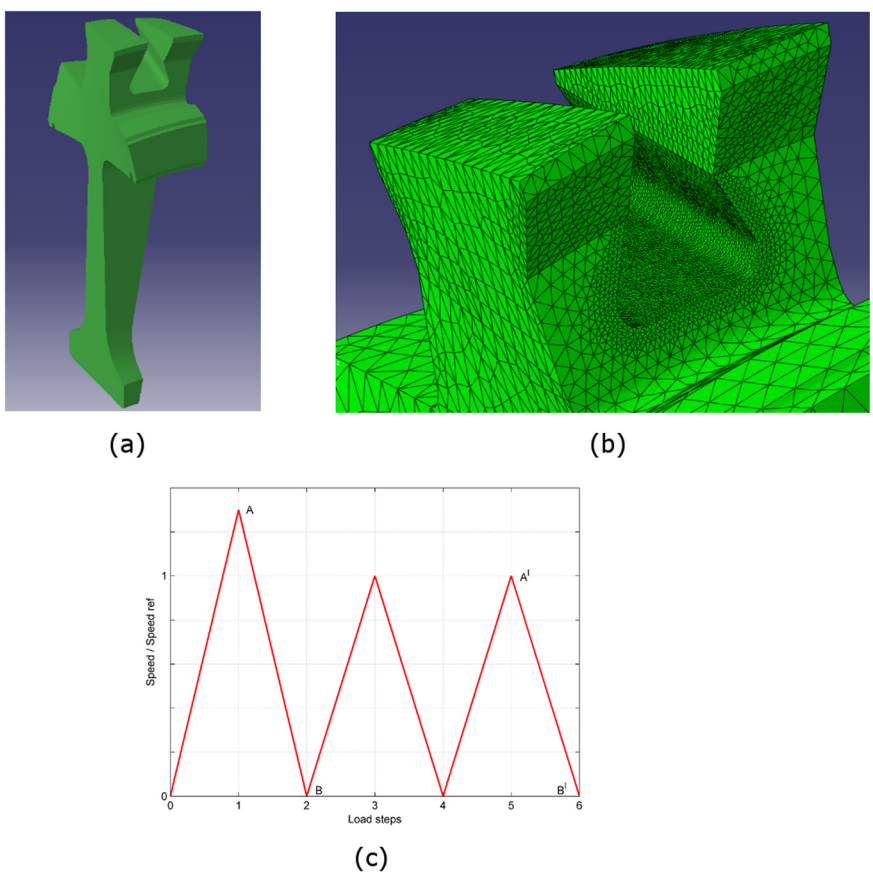

FIG. 2 FEM results of the disk sector: (*a*) stress-strain behavior, (*b*) plastic strain field.

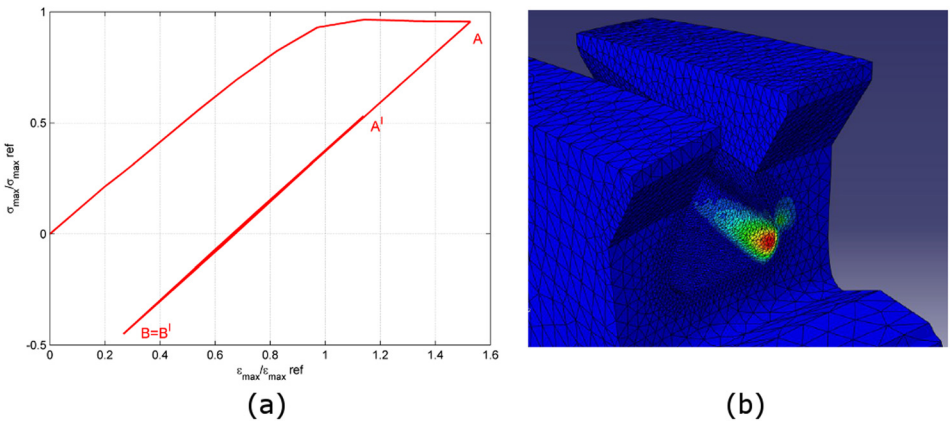

COMPANION SPECIMENS

To experimentally reproduce the stress–strain field experienced by the disk, a notched specimen has been designed (**Fig. 3**). The specimen must be able to repro-duce, under a uniaxial load in $R = 0$ condition, the same equivalent plastic strain (*PEEQ*) field induced by the first load cycle and the maximum principal stress (σ_{max}) experienced by the disk in the following cycles. In order to fulfill these con-ditions, different specimen geometries have been analyzed. Good agreement with the stress state in the disk has been reached using a specimen with a semicircular notch with a 9 mm radius onto a 30 by 18 mm rectangular section (**Fig. 3**). Speci-men length is equal to 200 mm. The comparisons between disk FE results and spec-imen, in terms of equivalent plastic strain (*PEEQ*) and maximum principal stress (σ_{max}), are shown in **Figs. 4(*b*)** and **4(*c*)**. The specimen geometry best reproduces the plastic gradient and the principal stress in the 30 mm deep direction. However, differences in terms of triaxiality between the disk and the companion specimen can be present.

FIG. 3 Specimen geometry and EDM micronotch orientation. All dimensions are expressed in millimeters.

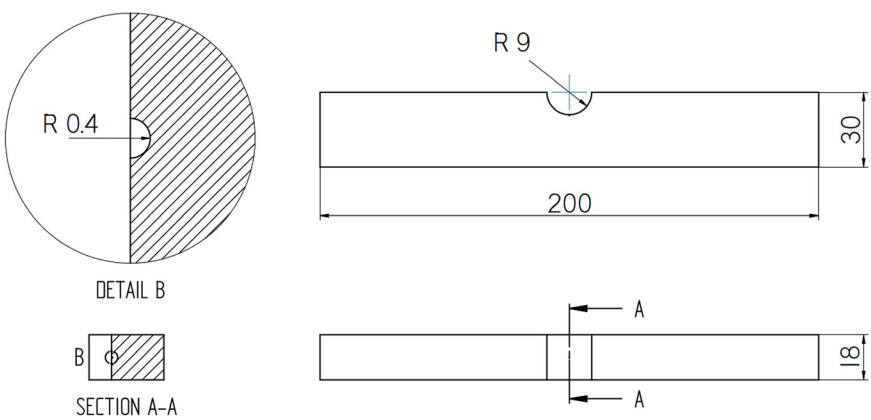

FIG. 4 Specimen design: (*a*) FEM model, (*b*) equivalent plastic strain field, (*c*) maximum principal stress field, (*d*) final geometry.

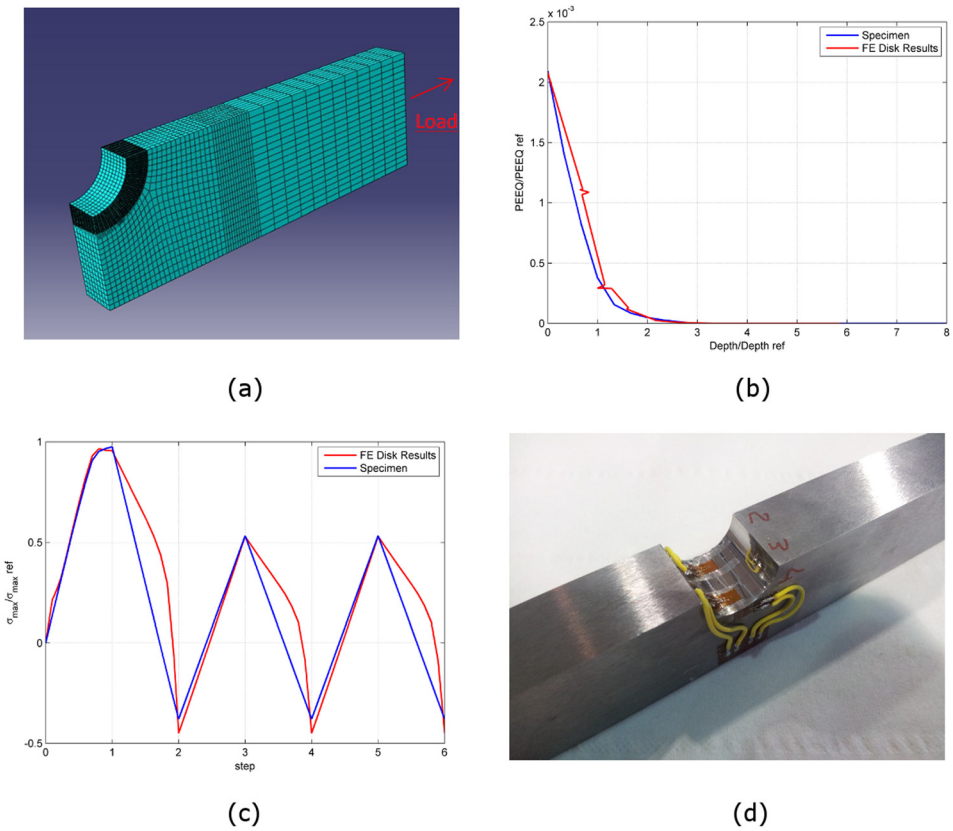

STABLE STRESS–STRAIN CYCLES AT THE SPECIMENS' NOTCH

Regarding the specimen, three different load conditions have been considered, as in **Fig. 5(*a*)**. In the first one (afterwards referred to as OL + BL) an initial overspeed, significantly higher than the nominal speed, has been considered followed by two cycles performed at the nominal speed, as shown in the FE results of disk. In the second case (afterwards referred to as BL), only the nominal speed has been modeled, whereas in the third (afterwards referred to as OL) only the overload speed has been reproduced. The second and the third load cases have been considered to show the effect of overspeed on the fatigue life and on the crack propagation. In the OL and BL load cases, 100 start-up and shut-down cycles have been simulated in order to check material stress/strain transient behavior.

The results of the FE analysis, in the OL + BL condition, are shown in **Fig. 5(*b*)**. The elastic shakedown condition is reached in the same way as already seen for the disk and the last load cycle has a stress ratio very close to $R = -1$, because of high residual stresses due to overload first cycle. Moreover, in the BL condition (**Fig. 5(*c*)**), the material reaches an elastic shakedown condition soon after the first load cycle. Due to the modest plastic deformation reached at the first load application and consequent lower residual stresses, the stabilized load cycle is close to a stress ratio

FIG. 5 Results of the FE analysis: (*a*) load conditions considered (*b*) with first overload (OL + BL), (*c*) only nominal speed (BL), and (*d*) only overload (OL).

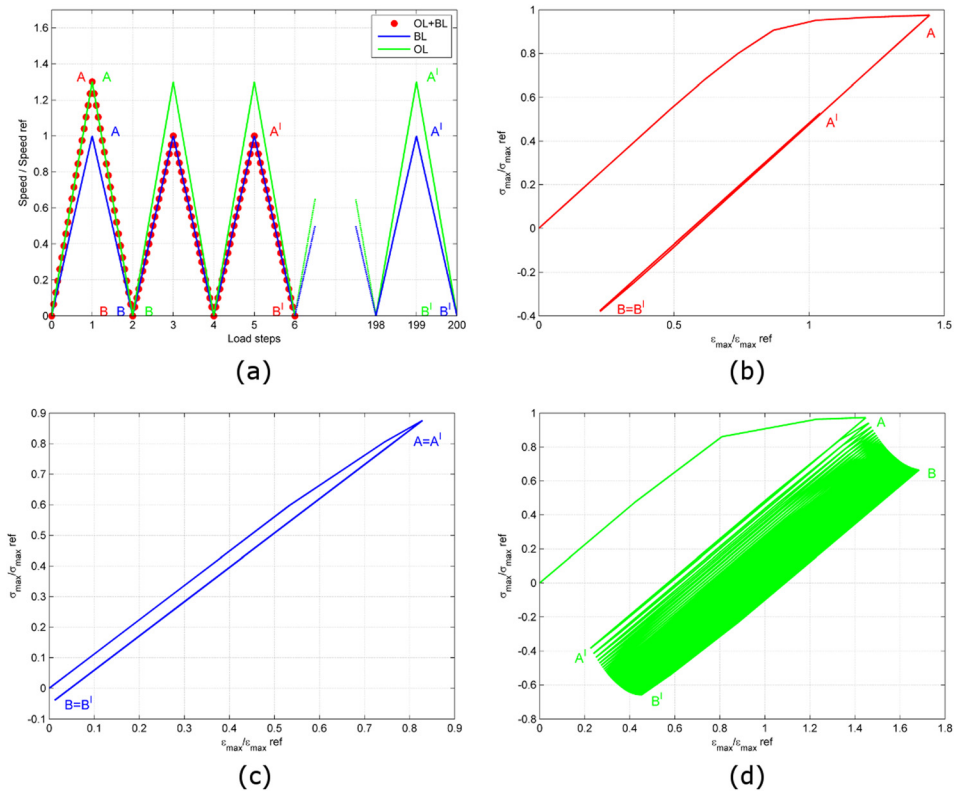

$R = 0$. In the OL case (loads corresponding to overspeed), the elastic shakedown condition is reached after some initial mean stress relaxation as can be seen in **Fig. 5(*d*)**: again the 100th cycle is stabilized and close to $R = -1$ stress ratio, as in the OL + BL case.

Fatigue Experiments Onto Companion Specimens

In order to simulate the presence of a defect, a small semi-circular electrical discharge machining (EDM) micronotch has been introduced at the deepest point of the semicircular notch, as depicted in **Fig. 3**.

Considering the typical resolution [10] of the magnetic particle inspection (MPI) technique commonly adopted for inspecting rotor disks (together with ultrasonic (US) scans), the depth of the defect has been set to $a_0 = 0.4$ mm (a detail of a micronotch is shown in **Fig. 6**).

A total of six uniaxial fatigue tests have been carried out: two for each of the three load cases considered. Tests have been carried out, using a servo-hydraulic load frame with 250 kN capacity, under load control at a frequency of 0.5 Hz. Each

FIG. 6
Specimen with defect and strain gauges.

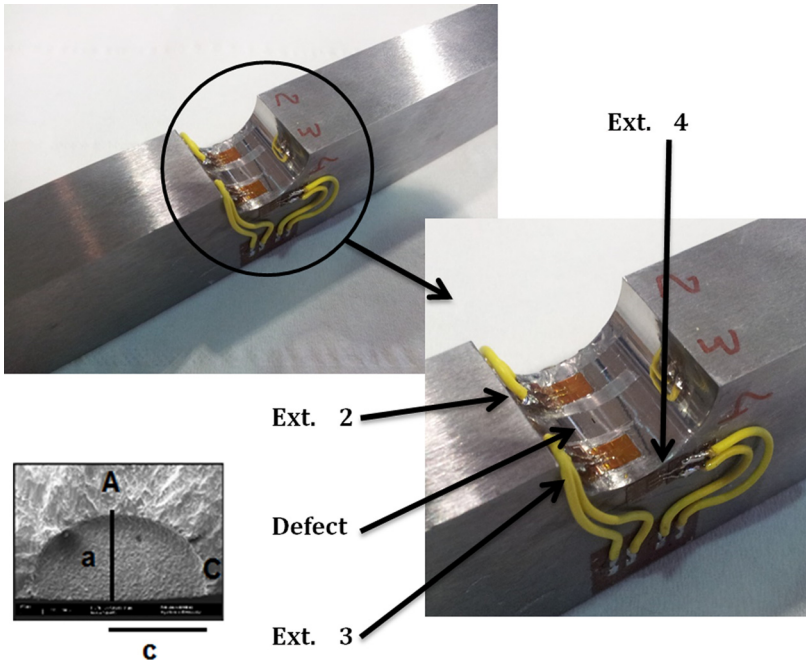

test has been regularly stopped to measure the crack length on the specimen surface through the plastic replication method [2], as shown in **Fig. 7(*a*)**. After the replicas had been removed from the specimen, they were analyzed using an optical microscope in order to measure the surface crack length $2c$, as shown in **Fig. 7(*b*)**. In **Fig. 7(*c*)**, the crack advance, in terms of surface crack length c versus number of cycles N, is shown. Starting from the crack length c, it has been possible to determine the discrete crack propagation rate as:

$$\frac{dc}{dn_i} \sim \frac{\Delta c}{\Delta N_i} = \frac{c_i - c_{i-1}}{N_i - N_{i-1}} \tag{1}$$

The results of the evaluation of crack growth rate (in terms of surface crack advance) are shown in **Fig. 7(*d*)**.

It can be seen that the propagation life in the OL + BL case is almost doubled with respect to BL. This fact shows the beneficial effect of the spinning tests. In the OL case (load cycles corresponding to start-ups up to overspeed), the propagation lifetime is approximately one-third of the BL one.

As shown in **Fig. 6**, all specimens were equipped with four strain gauges (gage length equal to 2.5 mm) to check the specimen alignment during the test and to record the force-strain response of the material in the 9 mm notch root during the test. All the gauges were positioned in order to measure axial strains. Experimental results are shown in **Fig. 8(*a*)** regarding the first few loading cycles of one of the OL + BL tests: experimental data (in terms of load versus strain at the notch root) confirm the shakedown condition that had been numerically predicted. This com-parison has not been possible for all the specimens and for the entire duration of the

FIG. 7 The replica technique and experimental data: (*a*) plastic replica technique, (*b*) optical microscope analysis, (*c*) crack length, and (*d*) crack growth rate.

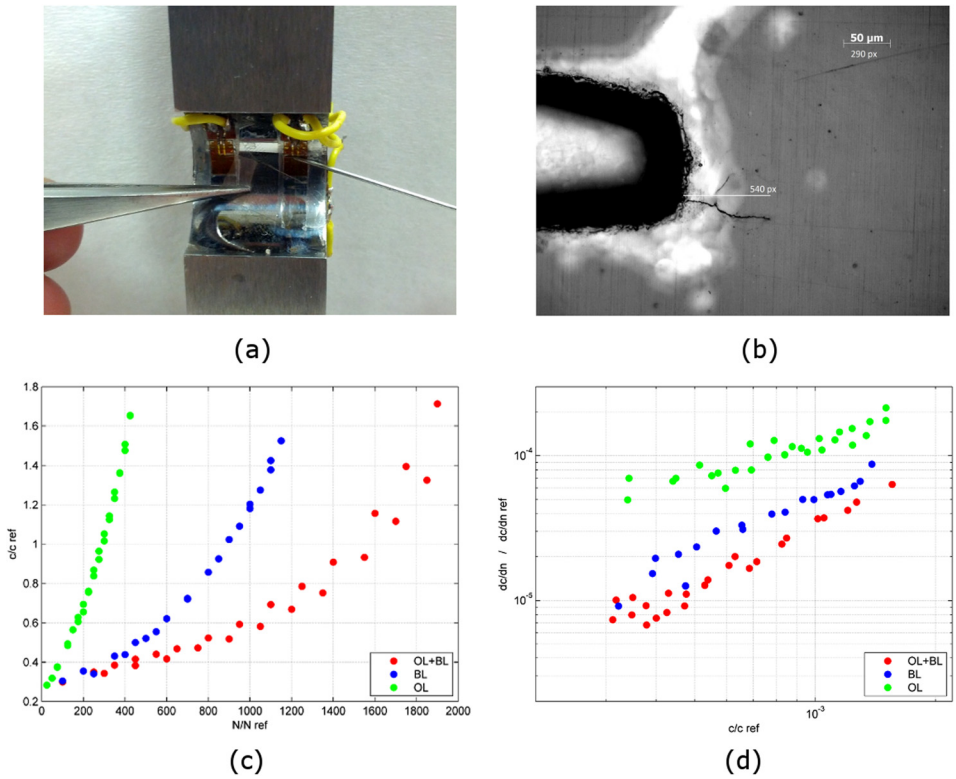

tests because of early gauge failures due to the high levels of force reached. At the end of the tests, each specimen was broken in liquid nitrogen to measure the crack shape (one of the cracks is shown in **Fig. 8(b)**). The average aspect ratio, a/c, measured at the end of the fatigue tests, was 0.9 for all the six specimens. This value was

FIG. 8 Specimen check. (*a*) Force-strain behavior during a OL + BL test, (*b*) crack shape at the end of a fatigue test.

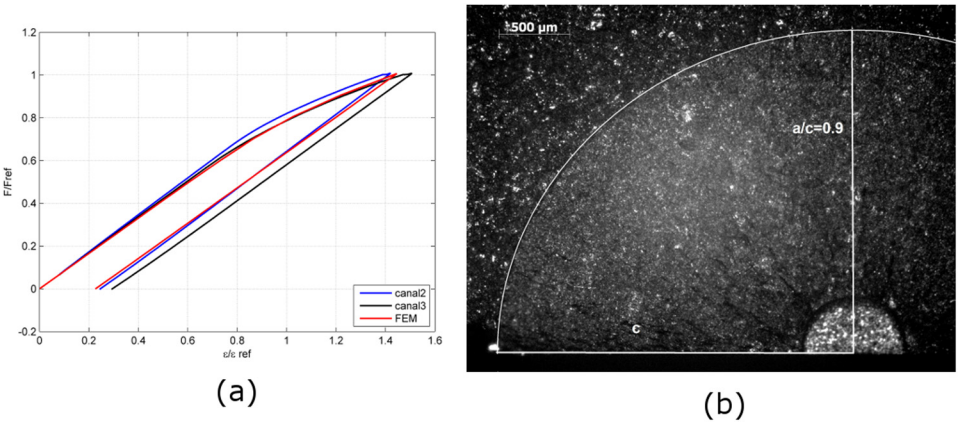

different from the initial shape factor, which was equal to 1 (semicircular EDM micronotch). The change of the crack shape during fatigue propagation was due to the different value of ΔK at the deepest point of the crack and at the surface. The relationship between a and c was calculated considering an elastic propagation of a semicircular surface crack. Stress intensity factor ranges at the crack deepest point and at the surface point were calculated according to the Newman–Raju expression [11]. Consequently, the experimental measurement of the surface crack length c allowed the direct estimation of the crack depth a during propagation experiments.

Fatigue Crack Growth Model

An EDM micronotch with a depth of 0.4 mm can be assumed to be a short crack, as in Ref. [12]. Due to elastic shakedown condition, the loading cycle of the short cracks is completely elastic, so that the fatigue life of the specimens can be treated as an initial nucleation/incubation and a consequent propagation [13].

We have taken the nucleation as minimum surface crack length needed to have a unique stable crack front around the initial defect, as schematically depicted in **Fig. 9**. By means of microscopic observations (at the specimen surface and at the bottom of the micronotch), the minimum crack advance for a stable propagation for the initial defect has been estimated between 50 and 80 μm, different for the three load cases:

$$\Delta c_{nuc} = \Delta a_{nuc} = 65 \pm 15\ \mu\text{m}$$

According to Feng and Gross [3], shakedown problems of cracked structures can be modeled in terms of the stress intensity factor K. Accordingly, the value of the SIF at crack tip has been calculated through a suitable weight function (WF). In particular, the stress intensity factor K at the deepest point A of the crack (as shown in the detail of **Fig. 6**) was expressed as:

$$K_A = \int_0^a h_A(x,a)\sigma(x)dx \tag{2}$$

where $h_A(x,a)$ is the WF by Wang and Lambert [5] for tip A of a semielliptical surface crack in a finite thickness plate. Similarly, the Stress Intensity Factor K at the surface point C (as depicted in the detail of **Fig. 6**) of the crack was:

$$K_C = \int_0^a h_C(x,a)\sigma(x)dx \tag{3}$$

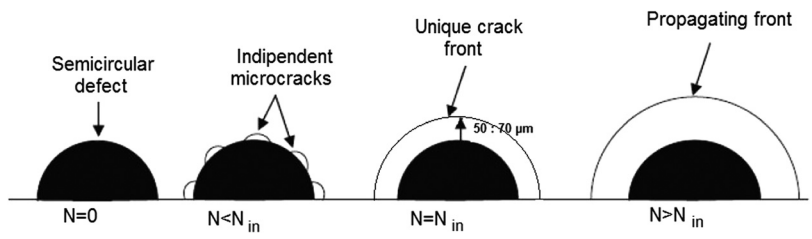

FIG. 9
Schematic of crack formation from the defect.

where $h_c(x,a)$ is again the WF for tip C of a surface semi-elliptical crack [5]. This WF was chosen because of the modest curvature of the notch with respect to crack size: a comparison with a series of elastic FE analyses onto semicircular cracks showed good predictions by Eqs 2–3 [14].

For applying Eqs 2–3, the stress distributions experienced by the specimen in the last loading cycle implemented in the FE analyses of the specimen (load steps A′ and B′) have been interpolated with appropriate polynomial functions, so that it has been possible to accurately calculate the $K_{\max}$ and $K_{\min}$ (corresponding to points A′ and B′, respectively).

Following the suggestions in Ref. [15], the load ratio R has been expressed as K ratio:

$$R = \frac{K_{\min}}{K_{\max}} \tag{4}$$

and the closure factor f, as in Ref. [16], as:

$$f = \frac{K_{op}}{K_{\max}} \tag{5}$$

so that

$$\Delta K_{eff} = K_{\max} - K_{op} = \frac{1-f}{1-R}\Delta K \tag{6}$$

Consequently, the crack growth rate at crack tips A and C was described as [17]:

$$\frac{da}{dN} = C_{07}.\Delta K_{i,eff}^{n_{07}} \tag{7}$$

where C_{07} and n_{07} are the parameters of the effective crack propagation curve, obtained testing the material at a load ratio R equal to 0.7. These parameters were obtained following the requirements proposed in the ASTM E647 standard.

The closure factor f was calculated through Newman's expressions [4] as:

$$f = \begin{cases} \max(R, H_0 + H_1 \cdot R + H_2 \cdot R^2 + H_3 \cdot R^3 & R \le 0 \\ H_0 + R \cdot H_1 & -2 \le R \le 0 \\ H_0 - 2 \cdot H_1 & R \le -2 \end{cases} \tag{8}$$

with:

$$H_0 = \left(0.825 - 0.34\alpha + 0.05\alpha^2\right) \cdot \left(cos\left(\frac{\pi\sigma_{max}}{2\sigma_0}\right)\right)^{1/\alpha}$$

$$H_1 = (0.415 - 0.071\alpha)\frac{\sigma_{max}}{\sigma_0} \tag{10}$$

$$H_2 = 1 - H_0 - H_1 - H_3 \tag{11}$$

$$H_3 = 2 \cdot H_0 + H_1 - 1 \tag{12}$$

where:

$\sigma_{\max}$ = the maximum stress during the loading cycle, and

α = the constraint factor described below.

The analytical model by Newman, which was developed for a through crack, provides satisfactory results even for semi-elliptical surface cracks, as described in Refs. [18,19]. Such an approach is also adopted to evaluate closure levels for surface cracks in the short crack propagation model proposed in the European SINTAP/FITNET Procedure [20].

Because of the complexity of the geometry of the specimen, as in Refs. [16,21], the normalized stress σ_{max}/σ_0 has been replaced with the normalized Stress Intensity parameter K_{max}/K_0:

$$f = function(K_0, K_{max}, \alpha) \tag{13}$$

where K_0 is the flow stress intensity factor, as in Refs. [16,22]. Different expressions have been proposed to define σ_0 [23–25], but because of the very high level of σ_{max}, it has taken the original Newman's formulation [23]:

$$\sigma_0 = \frac{R_m + R_{p02}}{2} \tag{14}$$

In order to determine the constraint factor, the plastic zone at the crack tip of a crack propagating from the EDM notch has been estimated by a series of FEM analyses. In particular, considering a semi-circular crack on the symmetry plane, we have modeled one-fourth of the specimen with the EDM micronotch and different prospective crack sizes, as shown in **Fig. 10**. The analyses have been run utilizing the same software and the same cyclic plasticity model previously mentioned. The constraint factor α at P_{max} was calculated as [26]:

$$\alpha = \frac{\int_{A_0} \sigma_n dA_n}{\sigma_0 A_0} \tag{15}$$

where:

σ_n = the stress in the nth yielded element of the plastic zone,
A_n = the projected area of the same element on the ligament, and
A_0 = the projected area of the whole plastic zone on the ligament.

FIG. 10 FEM model for the calculation of constraint factor α: (*a*) refined mesh at the crack tip, (*b*) plastic zone at the crack tip at the max load (stabilized cycle).

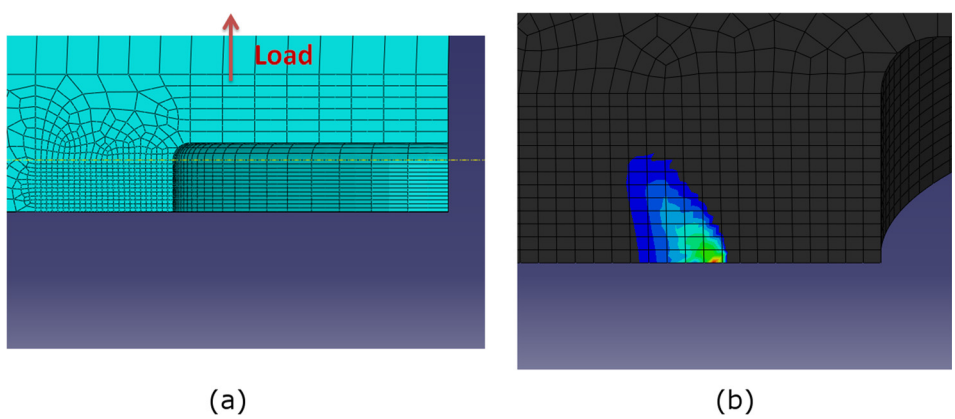

TABLE 1

Constraint factor—α—calculated through FE analyses for the OL + BL load case.

$\frac{a}{a\,ref}$	α
0.17	1.38
0.3	1.49
0.6	1.65
$\bar{\alpha} = \alpha_{mean}$	1.51

The analyses have been carried out for different crack depths and for all the three load cases. In **Table 1** the results of α, for the case OL + BL, are reported. The influence of the parameter α on life prediction is generally low, as depicted in **Fig. 11** for the OL + BL case. Consequently, for the crack growth simulations, an average value $\bar{\alpha}$ was considered to correctly represent the constraint factor in the whole crack propagation.

A propagation algorithm has been implemented to iteratively calculate crack advance for the two crack tips from initial crack length:

$$a_{\text{start}} = c_{\text{start}} = a_0 + \Delta a_{nuc} \tag{16}$$

and then:

$$\begin{cases} a_{i+1} = a_i + da = a_i + \dfrac{da}{dN}\Delta N \\ c_{i+1} = c_i + dc = c_i + \dfrac{dc}{dN}\Delta N \end{cases} \tag{17}$$

The comparisons between prediction and experimental data (expressed in terms of the estimated crack depth) are shown in **Fig. 12(*a*)** (crack growth rate) and **Fig. 12(*b*)** (crack depth). In the crack growth calculations, the predicted crack aspect ratio has been approximately 0.92, close enough to the average experimental value.

FIG. 11

Influence of the constraint factor α on the life prediction in OL + BL case.

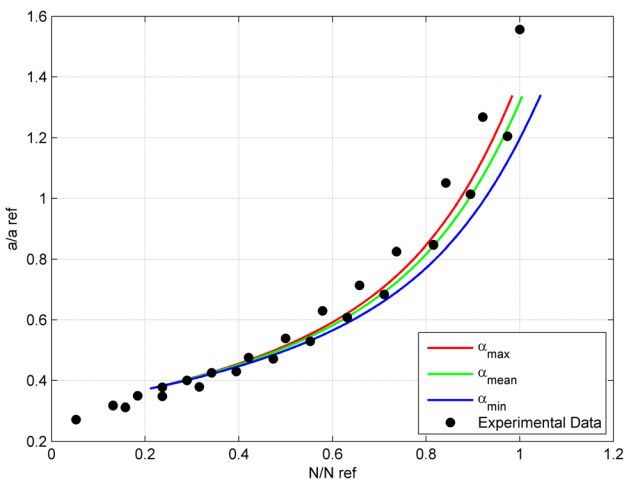

FIG. 12 Crack growth model results: (*a*) crack growth rate and (*b*) crack length.

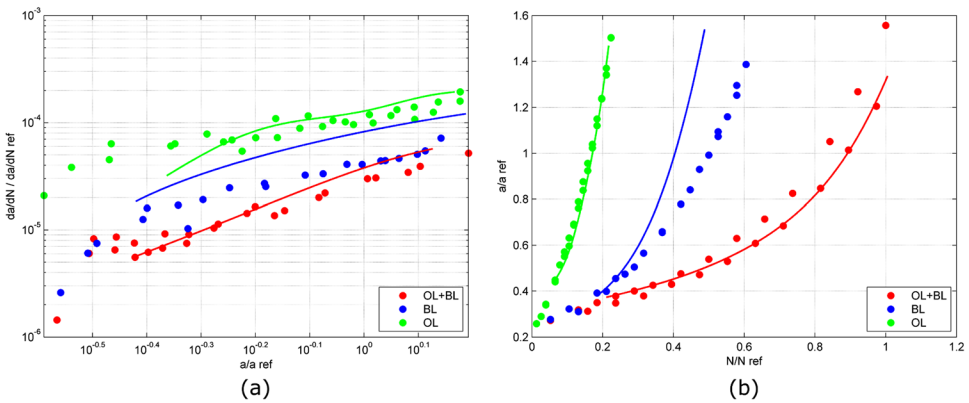

Discussion

The BL case is the one where the predictions are far from the experiments (the difference between model and tests is 40 % of lifetime), while the OL + BL and OL cases are described very well by the crack growth model.

This behavior can be explained considering that Newman's *f* factor, as discussed in Ref. [27], is not very precise when K_{max} is similar to the limit K_o: this happens in the BL case, where the plastic strain field is very low and the maximum value of σ_{max} is close to the limit σ_0, resulting in less accurate predictions. In OL + BL and OL cases, the residual compression stress fields in the elastic-shakedown condition significantly decreases the maximum value K_{max} reached during the cyclic load with respect to the BL case.

Moreover, it is worth remarking that the ΔK cycles under OL + BL loads are less severe than the ones under BL, because the stress ratio similar to a $R = -1$ condition instead of the $R = 0$ stress ratio of the BL case (this effect can be appreciated also from **Fig. 5**). This is the likely reason why the propagation lifetime period of the specimens is approximately 50 % greater in the OL + BL with respect to BL.

Conclusion

Three different loading conditions of the blade attachment of a turbine disk have been studied: the first one with loads at nominal speed condition (BL), the second with an initial overload prior to base-load (OL + BL) and the third one with loads corresponding to over-speed (OL). The stress–strain behavior, numerically evaluated, has been experimentally reproduced using a notched specimen with the same PEEQ of the blade attachment.

A series of crack growth tests were performed on the notched specimens with an additional 0.4 mm EDM micronotch in order to simulate the presence of a potential microdefect. The experiments have shown that the residual stress field induced by the OL is able to significantly increase the fatigue life of the notched specimens.

A crack propagation algorithm based upon the Newman's closure function and the estimation of SIF by a WF applied to elastic shakedown stress field has been able

to accurately predict crack growth rate for two series of experiments (OL + BL, OL) where there is a significant stress shakedown. In the case of BL loads, the effect of residual stresses are negligible: the very high stresses (close to the flow stress) make the prediction conservative with respect to the experiments.

ACKNOWLEDGMENTS

The present activity has been carried out within a research contract between AEN (Genova, Italy) and Politecnico di Milano, Dipartimento di Meccanica (Milano, Italy). The research has been devoted to developing tools and methods for the flaw tolerant design and life prediction of turbine disks.

References

[1] Schjive, J., *Fatigue of Structures and Materials*, Kluwer Academic Publishers, Dordrecht, the Netherlands, 2004.

[2] Larsen, J. M. and Allison, J. E., Eds., *Small-Crack Test Methods, ASTM STP 1149*, American Society for Testing and Materials, Philadelphia, PA, 1992.

[3] Feng, X.-Q. and Gross, D., "A Global/Local Shakedown Analysis Method of Elasto-plastic Cracked Structures," *Eng. Fract. Mech.*, Vol. 63, No. 2, 1999, pp. 179–192.

[4] Newman J. C., "A Crack Opening Stress Equation for Fatigue Crack Growth," *Int. J. Fatigue*, Vol. 24, No. 4, 1984, pp. 131–135.

[5] Wang X. and Lambert, S. B., "Semi-Elliptical Surface Cracks in Finite-Thickness Plates With Built-In Ends. II. Weight Function Solutions," *Eng. Fract. Mech.*, Vol. 68, No. 16, 2001, pp. 1743–1754.

[6] Madia, M., Beretta, S., Foletti, S. and Cavalleri, E. A., "A Tool for the Structural Integrity Assessment of Turbine Disks: Probabilistic and Numerical Background," *Proceedings of the ASME TurboExpo 2013 Conference*, San Antonio, TX, June 3–7, 2013.

[7] Voce, E., "A Practical Strain-Hardening Function," *Metallurgica*, Vol. 51, 1955, pp. 219–226.

[8] Chaboche, J. L., "Constitutive Equations for Cyclic Plasticity and Cyclic Viscoplasticity," *Int. J. Plast.*, Vol. 5, No. 3, 1989, pp. 247–302.

[9] König, J. A., *Shakedown of Elastic-Plastic Structures*, Elsevier, Amsterdam, 1987.

[10] Georgiu, G. A., "Probability of Detection (PoD) Curves: Derivation, Applications and Limitations," *HSE Research Report 454*, HSE, London, 2006.

[11] Newman, J. C. and Raju, I. S., "Stress-Intensity Factor Equations for Cracks in Three-Dimensional Finite Bodies," *NASA Technical Memorandum 83200*, NASA, Washington, D.C., 1981.

[12] Savaidis, G., Savaidis, A., Tsamasphyros, G. and Zhang, C., "On Size and Technological Effects in Fatigue Analysis and Prediction of Engineering Materials and Components," *Int. J. Mech. Sci.*, Vol. 44, No. 5, 2002, pp. 521–543.

[13] Santus, C. and Taylor, D., "Physically Short Crack Propagation in Metals During High Cycle Fatigue," *Int. J. Fatigue*, Vol. 31, Nos. 8–9, 2009, pp. 1356–1365.

[14] Scaccabarozzi, F., 2013, "Valutazione Della Durata a Fatica di Dischi per Turbine a Gas Tramite Prove Sperimentali e Modelli di Propagazione in Campo Elasto-Plastico," M.Sc. thesis, Politecnico di Milano, Milan, Italy (in Italian).

[15] Huang, X. and Moan, T., "Improved Modeling of the Effect of *R*-ratio on Crack Growth Rate," *Int. J. Fatigue*, Vol. 29, No. 4, 2007, pp. 591–602.

[16] McClung, R. C., "Finite Element Analysis of Specimen Geometry Effects on Fatigue Crack Closure," *Fatigue Fract. Eng. Mater. Struct.*, Vol. 17, No. 8, 1994, pp. 861–872.

[17] Elber, W., "Fatigue Crack Closure Under Cyclic Tension," *Eng. Fract. Mech.*, Vol. 2, No. 1, 1970, pp. 37–45.

[18] Vormwald, M. and Seeger, T., "The Consequences of Short Crack Closure on Fatigue Crack Growth Under Variable Amplitude Loading," Fatigue Fract. Eng. Mater. Struct., Vol. 14, Nos. 2/3, 1991, pp. 205–225.

[19] McClung, R. and Sehitoglu, H., "Closure Behavior of Small Cracks Under High Strain Fatigue Histories," *Mechanics of Fatigue Crack Closure*, J. Newman and W. Elber, Eds., ASTM International, Philadelphia, PA, 1988, pp. 279–299.

[20] Zerbst, U., Schodel, M., Webster, S. and Ainsworth, R., Fitnet-for-Service Fracture Assessment of Structures Containing Cracks. A Workbook Based on the European SINTAP/FITNET Procedure, Elsevier Science, Amsterdam, 2007.

[21] Beretta, S., Carboni, M. and Madia, M., "Modelling of Fatigue Thresholds for Small Cracks in a Mild Steel by "Strip-Yield" Model," *Eng. Fract. Mech.*, Vol. 76, No. 10, 2008, pp. 1548–1561.

[22] Liu, J. Z. and Wu, X. R., "Study on Fatigue Crack Closure Behavior for Various Cracked Geometries," *Eng. Fract. Mech.*, Vol. 57, No. 5, 1997, pp. 475–491.

[23] Newman, J. C., "A Crack Closure Model for Predicting Fatigue Crack Growth Under Aircraft Spectrum Loading," *Methods and Models for Predicting Fatigue Crack Growth Under Random Loading*, J. B. Chang and C. M. Hudson, Eds., ASTM International, Philadelphia, PA, 1981, pp. 53–84.

[24] Savaidis, G., Dankert, M. and Seeger, T., "An Analytical Procedure for Predicting Opening Loads of Cracks at Notches," *Fatigue Fract. Eng. Mater. Struct.*, Vol. 18, No. 4, 1995, pp. 425–442.

[25] McClung, R. C. and Sehitoglu, H., "Characterization of Fatigue Crack Growth in Intermediate and Large Scale Yielding," *J. Eng. Mater. Technol.*, Vol. 113, No. 1, 1991, pp. 15–22.

[26] Newman, J. C., Bigelow, C. A., and Shivakumar, K. N., "Three-Dimensional Elastic–Plastic Finite-Element Analyses of Constraint Variations in Cracked Bodies," *Eng. Fract. Mech.*, Vol. 46, No. 1, 1993, pp. 1–13.

[27] Newman, J. C. and Ruschau, J. J., "The Stress-Level Effect on Fatigue-Crack Growth Under Constant-Amplitude Loading," *Int. J. Fatigue*, Vol. 29, No. 9, 2007, pp. 1608–1615.